



Calculations of Dielectronic Recombination and Electron-impact Excitation Rate Coefficients of Highly Charged Sulfur Ions

D. H. Zhang¹, Z. W. Wu¹, C. Ren¹, J. Jiang¹, L. Y. Xie¹, R. Schuch², J. M. Zhang¹, and C. Z. Dong¹

¹ Key Laboratory of Atomic and Molecular Physics and Functional Materials of Gansu Province, College of Physics and Electronic Engineering, Northwest Normal University, Lanzhou 730070, People's Republic of China; zhongwen.wu@nwnu.edu.cn, dongcz@nwnu.edu.cn.

² Department of Physics, Stockholm University, AlbaNova University Center, SE-10691 Stockholm, Sweden

Received 2019 July 3; revised 2019 December 17; accepted 2020 January 8; published 2020 March 5

Abstract

Connected to the experiment performed at the Stockholm electron beam ion trap, a systematic relativistic configuration-interaction calculation is carried out to compare with the experimental spectra. In particular, separate rate coefficients are calculated for dominant recombination and excitation processes in the range of the impact electron energy determined by the experiment. By means of the relevant experimental parameters, the presently calculated dielectronic recombination rate coefficients for S^{15+} and S^{14+} ions and electron-impact excitation ones for S^{15+} , S^{14+} , and S^{13+} ions are employed further to synthesize overall theoretical spectra for comparison with the experimentally measured spectra. Overall, very good agreements with the experimental results are found except for one missing excitation peak around the impact electron energy 2.52 keV, which cannot be explained by the present calculations and thus remains open.

Unified Astronomy Thesaurus concepts: [Dielectronic recombination \(2061\)](#); [Theoretical models \(2107\)](#); [Excitation rates \(2067\)](#)

1. Introduction

A large amount of matter in the universe is composed of plasma, which contains electrons and highly charged ions (HCI). Therefore, collision processes of electrons with HCI are among the most common processes in astrophysical plasmas. These collision processes have a very important influence on charge state distribution of HCI and also on formation mechanism of the corresponding spectral emissions (Wu et al. 2012). Dielectronic recombination (DR) is a two-step resonant process, in which a free electron is captured by a target ion with a simultaneous excitation of one of its bound electrons, followed by a radiative stabilization of the produced doubly excited state to an energetically lower state. Since Massey and Bates first proposed the DR process 70 yr ago (Massey & Bates 1942), a great deal of relevant work has been performed in both theory and experiment (Burgess 1964; Andersen et al. 1989; Knapp et al. 1989; Kilgus et al. 1990). Besides the DR process, another significant inelastic collision process of electrons with HCI is the electron-impact excitation (EIE), in which a target ion is excited to some energetically higher state by impact of a free electron. Likewise, many theoretical and a limited number of experimental studies have been carried out on the EIE process (Crandall et al. 1974; Chang 1975; Williams & Boziniš 1975; Hagelstein 1986; Lafyatis & Kohl 1987; Chantrenne et al. 1992; Wong et al. 1995; Zhang & Pradhan 1995; Wu et al. 2011; Piwiński et al. 2018; Ren et al. 2018). Moreover, DR and EIE rate coefficients are essentially necessary for properly modeling various astrophysical and laboratory plasmas (Kunze & Johnston 1971; Gu 2003; Shen et al. 2007; Wu et al. 2015; Badnell et al. 2016).

It is well known that sulfur is one of the most abundant elements in the solar system, and highly charged sulfur ions are widely present in high-temperature astrophysical and laboratory plasmas (Anders & Grevesse 1989; Cassam-Chenai et al. 2004; Hwang et al. 2004). Furthermore, sulfur also exists as an impurity in many alloys that are utilized in fusion devices and

its emission lines are therefore present in the spectra from such plasmas. In recent times, an enormous amount of data collected by space-based observatories such as the *XMM-Newton* and *Chandra* highlights the need of highly accurate atomic data for astrophysical studies (Cassam-Chenai et al. 2004; Hwang et al. 2004; Foster et al. 2010). The new X-ray space missions, e.g., the 2017 launched Japanese *Hitomi* (Astro-H) and the 2018 launched Chinese Hard X-ray Modulation Telescope, probe higher temperature and dense astrophysical plasmas, where the data for high- Z ions such as S, Ca, Ti, Fe, and Ni are needed (Ishisaki et al. 2018; Takahashi et al. 2018). Accurate atomic data of sulfur and its ions such as energy levels, DR and EIE cross sections and rate coefficients are thus needed for the diagnosis and modeling of the emission lines and of these astrophysical and laboratory plasmas (Deb & Hibbert 2006). As the simplest ionic systems in collisionally ionized plasmas, hydrogenlike and heliumlike (sulfur) ions are of particular interest as the line ratios of their radiative transitions can be readily used for plasma diagnosis (Pradhan & Shull 1981; Smith et al. 2001; Porquet et al. 2002). Moreover, reliable atomic data of their isoelectronic sequences are also needed for the same purpose (Foster et al. 2010; Porquet et al. 2010).

The purpose of the present work is to develop a proper theoretical procedure for calculating the DR and EIE rate coefficients and to test it by comparison with experimental data. Mahmood et al. (2012) measured DR and EIE rate coefficients of highly charged few-electron ions at the Stockholm refrigerated electron beam ion trap (EBIT). The DR rate coefficients were obtained by detecting the charge state distribution of highly charged few-electron ions with a newly developed time-of-flight technique. In addition to the DR time-of-flight spectra, the X-ray spectra, produced mainly following the DR and EIE processes, were also collected. The combination of these two kinds of measurements allowed them to separate the DR and EIE spectra, and the EIE rate coefficients for summed intensities with known fractions of highly charged few-electron ions were extracted. In order to check the

consistency of theory with the experimentally measured spectra, they also calculated KLL and KLM DR rate coefficients of hydrogenlike S^{15+} ions by using the relativistic many-body perturbation theory. Admittedly, such an experimental method would enable the extraction of DR and EIE rate coefficients for specific charge states, and thus has promising prospects for further studies of the DR and EIE processes at electron beam ion traps.

In the present work, we systematically calculate the DR and EIE rate coefficients. For doing so, we first employ the flexible atomic code (FAC; Gu 2008) to produce energy levels, radiative rates, Auger rates, and cross sections. By comparing with available experimental and NIST results (Ali et al. 2011; Kramida et al. 2019), excellent agreements are obtained for the DR resonance energies and EIE excitation energies of S^{15+} , S^{14+} , and S^{13+} ions. Finally, these atomic data are further utilized to calculate the rate coefficients, and further to check the developed theoretical procedure by comparing with the experimental results.

This paper is structured as follows. In the next section, the theoretical method for the calculations of the DR and EIE rate coefficients is described. In Section 3, we present the presently calculated DR and EIE rate coefficients, and compare them with the experimentally measured results. In the end, a brief conclusion of the present work is given in Section 4.

2. Theoretical Method

In general, the rate coefficients $\alpha(\varepsilon_e)$ of a particular electron-impact process are related to the corresponding cross sections σ as follows (Shore 1969),

$$\alpha(\varepsilon_e) = \int \sigma v f(v) dv. \quad (1)$$

Here, ε_e is the kinetic energy of the impact electrons and $f(v)$ denotes an anisotropic velocity distribution of electrons. Moreover, the integration over v runs from 0 to the positive infinity $+\infty$. Below, we shall explain how to calculate the DR and EIE cross sections in order to obtain the corresponding rate coefficients.

2.1. Dielectronic Recombination

As stated above, the DR process can be expressed as

$$A^{q+} + \varepsilon e \rightarrow [(A^{(q-1)+}]^{**} \rightarrow [(A^{(q-1)+}]^* + h\nu, \quad (2)$$

where A^{q+} denotes the initial target ion of the first-step resonant capture process, $[(A^{(q-1)+}]^{**}$ the resonant doubly excited state, and $[(A^{(q-1)+}]^*$ the final target ion of the second-step radiative decay process, which could be in any bound state energetically lower than its ionization threshold. The DR cross section from an initial state i to a final state f via an intermediate doubly excited state d can be well approximated as a function of the impact electron energy ε_e as follows (Shore 1969),

$$\sigma(\varepsilon_e) = \frac{1}{\pi} S \frac{\Gamma/2}{(E_{di} - \varepsilon_e)^2 + \Gamma^2/4}. \quad (3)$$

In this approximation, the natural width Γ of the doubly excited state d has been assumed to be smaller than the impact electron energy ε_e . E_{di} denotes the energy separation of the doubly excited state d with respect to the initial state i , i.e., the DR

resonance energy. Moreover, S represents an integrated DR cross section, that is, the DR strength, which is proportional to the capture rate $A^a(d \rightarrow i)$ into the doubly excited state d and also to the probability of the state d decaying radiatively to a nonautoionizing state (Kilgus et al. 1992),

$$S = \frac{g_d \pi^2 \hbar^3}{2g_i m_e E_{di}} \frac{A^a(d \rightarrow i) A^r(d \rightarrow f)}{\sum_k A^a(d \rightarrow k) + \sum_{f'} A^r(d \rightarrow f')}. \quad (4)$$

Here, g_i and g_d are the statistical weights of the initial and intermediate states. \hbar is the reduced Planck constant, and m_e is the mass of electrons. A^a and A^r denote, respectively, the autoionization and radiative decay rates. The radiative decay rate A^r is given by (Grant 1974; Dyall et al. 1989)

$$A^r = \frac{4e^2 w_p}{3\hbar c^3} |\langle \Psi_d | T^{(l)} | \Psi_f \rangle|^2, \quad (5)$$

where Ψ_d and Ψ_f are atomic state functions (ASFs) for the states d and f , respectively. e is the electron charge, c is the speed of light, and w_p is the energy of the decay photons. $T^{(l)}$ denotes the multipole radiative tensor operator. Moreover, the autoionization (Auger) decay rate can be given by

$$A^a = \frac{2\pi}{\hbar} |\langle \Psi_d | V_{\text{Coul}} | \Psi_i \rangle|^2. \quad (6)$$

Similarly, Ψ_i represents the ASF of the combined system ‘‘the initial target ion state plus the impact electron.’’ $V_{\text{Coul}} = 1/r_{pq}$ denotes the Coulomb operator describing the electron–electron interaction. It should be noted here that the Breit interaction among electrons hardly contributes to the energy level structure as well as DR and EIE of light atoms or ions such as sulfur ions considered in the present work and, thus, is not taken into account in the theoretical calculations.

2.2. Electron-impact Excitation

The EIE of ions consists of direct and resonant excitation processes. For the direct excitation process from an initial state ψ_i to a final state ψ_f of target ions, the corresponding cross section $\sigma_{\varepsilon_e}^{\text{dir}}(\psi_i \rightarrow \psi_f)$ can be expressed in terms of the collision strength $\Omega_{\varepsilon_e}^{\text{dir}}(\psi_i \rightarrow \psi_f)$ as

$$\sigma_{\varepsilon_e}^{\text{dir}}(\psi_i \rightarrow \psi_f) = \frac{\pi a_0^2}{k_e^2 g_i} \Omega_{\varepsilon_e}^{\text{dir}}(\psi_i \rightarrow \psi_f). \quad (7)$$

In this expression, a_0 is the Bohr radius, and g_i is the statistical weight of the initial state ψ_i . The relativistic wave number k_e of the impact electron is related to its kinetic energy ε_e by

$$k_e^2 = 2\varepsilon_e \left(1 + \frac{\alpha^2 \varepsilon_e}{2} \right) \quad (8)$$

with the fine structure constant α . Moreover, the collision strength $\Omega_{\varepsilon_e}^{\text{dir}}(\psi_i \rightarrow \psi_f)$ can be expressed as

$$\begin{aligned} \Omega_{\varepsilon_e}^{\text{dir}}(\psi_i \rightarrow \psi_f) &= 2 \sum_{\kappa_e \kappa_{e'}} \sum_{J_T} (2J_T + 1) \\ &\quad \times |\langle \psi_i \kappa_e, J_T M_T | V_{\text{Coul}} | \psi_f \kappa_{e'}, J_T M_T \rangle|^2. \end{aligned} \quad (9)$$

Here, ψ_{κ_e} and $\psi_{\kappa_{e'}}$ denote the wavefunctions of the incident and scattered electrons, respectively. J_T and M_T are total angular

Table 1
The Particular DR Processes of S¹⁵⁺ and S¹⁴⁺ Ions Considered in the Present Calculations

Initial Resonances	Doubly Excited Resonances	Final Resonances
1s (H-like S ¹⁵⁺)	2l2l 2l3l 2l4l 2l5l 2l6l 2l7l 2l8l 2l9l 2l10l	1s2l 1s2l 1s3l 2l2l 1s2l 1s4l 2l2l 2l3l 1s2l 1s5l 2l2l 2l3l 2l4l 1s2l 1s6l 2l2l 2l3l 2l4l 2l5l 1s2l 1s7l 2l2l 2l3l 2l4l 2l5l 2l6l 1s2l 1s8l 2l2l 2l3l 2l4l 2l5l 2l6l 2l7l 1s2l 1s9l 2l2l 2l3l 2l4l 2l5l 2l6l 2l7l 2l8l 1s2l 1s10l 2l2l 2l3l 2l4l 2l5l 2l6l 2l7l 2l8l 2l9l
1s ² (He-like S ¹⁴⁺)	1s2l2l 1s2l3l 1s2l4l 1s2l5l 1s2l6l 1s2l7l 1s2l8l 1s2l9l 1s2l10l	1s ² 2l 1s ² 2l 1s ² 3l 1s2l2l 1s ² 2l 1s ² 4l 1s2l2l 1s2l3l 1s ² 2l 1s ² 5l 1s2l2l 1s2l3l 1s2l4l 1s ² 2l 1s ² 6l 1s2l2l 1s2l3l 1s2l4l 1s2l5l 1s ² 2l 1s ² 7l 1s2l2l 1s2l3l 1s2l4l 1s2l5l 1s2l6l 1s ² 2l 1s ² 8l 1s2l2l 1s2l3l 1s2l4l 1s2l5l 1s2l6l 1s2l7l 1s ² 2l 1s ² 9l 1s2l2l 1s2l3l 1s2l4l 1s2l5l 1s2l6l 1s2l7l 1s2l8l 1s ² 2l 1s ² 10l 1s2l2l 1s2l3l 1s2l4l 1s2l5l 1s2l6l 1s2l7l 1s2l8l 1s2l9l

2l (l = s, p); 3l (l = s, p, d); 4l (l = s, p, d, f); 5l (l = s, p, d, f, g); 6l (l = s, p, d, f, g, h); 7l (l = s, p, d, f, g, h, i);
8l (l = s, p, d, f, g, h, i, k); 9l (l = s, p, d, f, g, h, i, k, l); 10l (l = s, p, d, f, g, h, i, k, l, m)

Note. The specific subshells included in the doubly excited resonances and final resonances of the processes are listed in the last row of the table.

momentum quantum number of the impact system “the target ion plus the impact electron” and its projection quantum number on the quantization axis chosen along the incident impact electrons, respectively.

Besides the direct impact excitation, the resonant excitation should also be considered. It is treated usually as a two-step process, i.e., resonant electron capture by an N -electron target ion (initial state i) to form an $(N+1)$ -electron doubly excited state d followed by autoionization to the final state f considered (Zhang & Sampson 2002). Under such a theoretical treatment, the resonant excitation cross section $\sigma_{\varepsilon_e}^{\text{res}}(\psi_i \rightarrow \psi_f)$ is given by (Badnell et al. 1991)

$$\sigma_{\varepsilon_e}^{\text{res}}(\psi_i \rightarrow \psi_f) = \frac{(2\pi a_0 I_H)^2 \tau_0}{\varepsilon_e} \sum_d \frac{g_d}{2g_i} A^a(d \rightarrow i) \times B(d \rightarrow f) L(\varepsilon_e). \quad (10)$$

In this equation, g_i and g_d denote the statistical weights of the initial state, i , and the doubly excited state, d , respectively, I_H is the ionization energy of hydrogen atoms, and $(2\pi a_0)^2 \tau_0 = 2.6741 \times 10^{-32} \text{ cm}^2 \text{ s}$. Moreover, B represents the branching ratio and is expressed as (Shore 1969)

$$B(d \rightarrow f) = \frac{A^a(d \rightarrow f)}{\sum_m A^a(d \rightarrow m) + \sum_{m'} A^r(d \rightarrow m')}, \quad (11)$$

where the radiative decay rate A^a and the autoionization rate A^r are given by Equations (5) and (6), respectively. In addition, $L(\varepsilon_e)$ in Equation (10) denotes a Lorentz profile of the impact electrons and is given by

$$L(\varepsilon_e) = \frac{1}{\pi} \frac{\Gamma/2}{(E_{di} - \varepsilon_e)^2 + \Gamma^2/4}. \quad (12)$$

With the direct impact excitation cross section (7) and the resonant excitation cross section (10) ready, one can easily give rise to total EIE cross section from the initial state ψ_i to the final

state ψ_f of target ions by summing over both of them as follows,

$$\sigma_{\varepsilon_e}(\psi_i \rightarrow \psi_f) = \sigma_{\varepsilon_e}^{\text{dir}}(\psi_i \rightarrow \psi_f) + \sigma_{\varepsilon_e}^{\text{res}}(\psi_i \rightarrow \psi_f). \quad (13)$$

Now, we are ready to employ Equations (1), (3), and (13) to calculate the DR and EIE rate coefficients. As seen from these equations, the calculations of the rate coefficients can be traced back to evaluate the DR resonance energies and EIE excitation energies as well as the radiative and autoionization decay rates. Below, the FAC is used to calculate these atomic date and finally to obtained the needed DR and EIE rate coefficients.

3. Results and Discussion

3.1. DR Rate Coefficients

In order to compare with the experimentally measured DR rate coefficients, the following dominant DR processes are considered in the present calculations,

$$\text{S}^{15+}(1s) + \varepsilon e \rightarrow [\text{S}^{14+}(2lnl (n = 2 - 20))]^{**} \rightarrow [\text{S}^{14+}]^* + h\nu, \quad (14)$$

$$\text{S}^{14+}(1s^2) + \varepsilon e \rightarrow [\text{S}^{13+}(1s2lnl (n = 2 - 20))]^{**} \rightarrow [\text{S}^{13+}]^* + h\nu, \quad (15)$$

$$\text{S}^{15+}(1s) + \varepsilon e \rightarrow [\text{S}^{14+}(3ln'l (n' = 3 - 20))]^{**} \rightarrow [\text{S}^{14+}]^* + h\nu, \quad (16)$$

$$\text{S}^{14+}(1s^2) + \varepsilon e \rightarrow [\text{S}^{13+}(1s3ln'l (n' = 3 - 20))]^{**} \rightarrow [\text{S}^{13+}]^* + h\nu. \quad (17)$$

In these DR processes of S¹⁵⁺ and S¹⁴⁺ ions, $1s2lnl$, $2lnl$, $1s3ln'l$, and $3ln'l$ represent the doubly excited states. To be more specific, in Table 1 we list the dominant intermediate doubly excited states and final states of the DR processes with $n(n') \leq 10$ only and $\Delta n = 1$ as given by Equations (14)–(15), while the ones for the DR with $\Delta n = 2$ expressed by

Table 2

The Presently Calculated Centroid (Resonance) Energies (in keV) Together with the Experimentally Measured Results (Ali et al. 2011) for the Particular DR Processes of S^{15+} and S^{14+} Ions

H-like S^{15+}			He-like S^{14+}		
Resonances	Centroid Energies		Resonances	Centroid Energies	
	Pres.	Exp.		Pres.	Exp.
2/2l	1.8267	1.825	1s2/2l	1.7524	1.752
2/3l	2.2799		1s2/3l	2.1531	2.154
2/4l	2.4301		1s3/4l	2.2891	
2/5l	2.4994		1s2/5l	2.3488	2.349
2/6l	2.5369		1s2/6l	2.3781	
2/7l	2.5598		1s2/7l	2.3974	
2/8l	2.5742		1s2/8l	2.4104	
2/9l	2.5844		1s2/9l	2.4198	
2/10l	2.5923		1s2/10l	2.4247	

Note. Exp.: (Ali et al. 2011).

Equations (16)–(17) are omitted for brevity. It should be noted that other DR channels with $n(n') \geq 20$ are neglected in the present calculations due to extremely weak contributions of them.

For illustrating the reliability and accuracy of the present theoretical results, the calculated peak centroid energies are listed in Table 2 together with experimental results (Ali et al. 2011) for comparison. It is found that the present results agree excellently with the experimental ones and the maximum relative discrepancy is within 0.1%. With such a comparison, these calculated atomic data such as energy levels and wavefunctions are utilized to evaluate the radiative and autoionization decay rates of the involved doubly excited states to all possibly energetically lower states. By assuming that every resonance of the doubly excited states involved follows a Lorentz distribution around its centroid, these decay rates are then employed further to calculate the corresponding DR cross sections with the use of Equations (3)–(4). Finally, the DR rate coefficients are obtained by convoluting the cross sections with a Gaussian velocity distribution of the incident impact electrons and the experimental full width at half maximum 24 eV (Ali et al. 2011; Mahmood et al. 2012).

In Figure 1, we show the presently calculated partial DR rate coefficients for dominant DR channels of S^{15+} and S^{14+} ions, which are compared with the experimentally measured results (Mahmood et al. 2012). The DR processes associated with the excitation of a K-shell electron to the L shell give rise to a series of strong peaks as labeled by the standard DR notations KLL, KLM, KLN, and KLO. The broad profile above the KLO peak arises from other DR processes that are listed in Table 1. By comparing with the experimental DR rate coefficients (Mahmood et al. 2012), the presently calculated results coincide very well with the experimentally measured ones with respect to both the resonance positions and the absolute strengths. Also the profiles of the theoretical and experimental DR rate coefficients agree very well with each other. From a theoretical point of view, the existing tiny discrepancy at the KLN of S^{14+} ions is likely the result of an incomplete consideration of the possible radiative cascades in the calculation of the branching ratio in Equation (4). This is because the branching ratio would be overestimated if the potential radiative decay channels are incompletely taken into account, which may ultimately give rise to overestimated DR

rate coefficients, as seen from Equations (1) and (3)–(4). Additionally, at higher energies, the DR resonances associated with $\Delta n = 2$ are also observed, that is accompanied with the excitation of a K-shell electron to the M shell (see Figure 1 inset). It can be seen that the DR processes with $\Delta n = 1$ are significantly larger than the ones with $\Delta n = 2$ for both S^{15+} and S^{14+} ions. Agreement for these higher- Δn resonances is reasonably good. The experimental results may also include other higher-order DR processes but they are not included in the present calculations.

For illustrating further the reliability of the present calculations on the DR rate coefficients, in Figure 2 we compare the presently calculated total DR rate coefficients of S^{15+} and S^{14+} ions with other available experimental (Mahmood et al. 2012) and theoretical results (Romanik 1988; Mazzotta et al. 1998; Gu 2003; Badnell 2006; Bautista & Badnell 2007). As can be seen clearly from the figure, the present total DR rate coefficients agree excellently well with these existing results. Although the present total DR rate coefficients for S^{14+} ions differ slightly from the experimental ones of Mahmood et al. (2012) around the electron energy 1.05 keV, they agree very well with the theoretical DR rate coefficients from all others. The total DR rate coefficients are obtained by means of the partial rate coefficients; therefore, these partial rate coefficients can be proven to be reliable. In order to enable a convenient application in astrophysical plasma modeling or a direct comparison for potential readers, moreover, we perform a fitting to the present total DR rate coefficients of S^{15+} and S^{14+} ions. The fitting formula utilized is given by (Wu et al. 2015)

$$\alpha^{\text{DR}}(kT_e) = (kT_e)^{-3/2} \sum_i^6 A_i e^{-B_i/kT_e}, \quad (18)$$

where A_i ($10^{-12} \text{ cm}^3 \text{ s}^{-1} (\text{eV})^{3/2}$) and B_i (eV) denote fitting parameters, which are listed in Table 3 for the presently calculated total DR rate coefficients of S^{15+} and S^{14+} ions. With the use of these fitting parameters, Equation (18) can be employed to reproduce total DR rate coefficients of S^{15+} and S^{14+} ions with discrepancies less than 0.1% and 0.6%, respectively.

3.2. EIE Rate Coefficients

We consider the direct and resonant EIE processes separately. As the experimental results in Mahmood et al. (2012) consist of a superposition of the EIE of sulfur ions with different charge states, we also consider the contribution from lithiumlike S^{13+} ions. The following direct excitation and corresponding radiative decay processes of S^{15+} , S^{14+} , and S^{13+} ions are considered in the present calculations,

$$\begin{aligned} S^{15+}(1s) + \epsilon e &\rightarrow [S^{15+}(nl(n=2-3))]^* + \epsilon' e \\ &\rightarrow [S^{15+}(1s)] + h\nu, \end{aligned} \quad (19)$$

$$\begin{aligned} S^{14+}(1s^2) + \epsilon e &\rightarrow [S^{14+}(1snl(n=2-3))]^* + \epsilon' e \\ &\rightarrow [S^{14+}(1s^2)] + h\nu \end{aligned} \quad (20)$$

$$\begin{aligned} S^{13+}(1s^22s) + \epsilon e &\rightarrow [S^{13+}(1s2lnl(n=3))]^* + \epsilon' e \\ &\rightarrow [S^{14+}(1s^22s)] + h\nu. \end{aligned} \quad (21)$$

The presently calculated excitation energies for these direct EIE processes of S^{15+} , S^{14+} , and S^{13+} ions are tabulated in Table 4 for comparison with other available results from NIST (Kramida et al. 2019). As seen clearly from the table, the

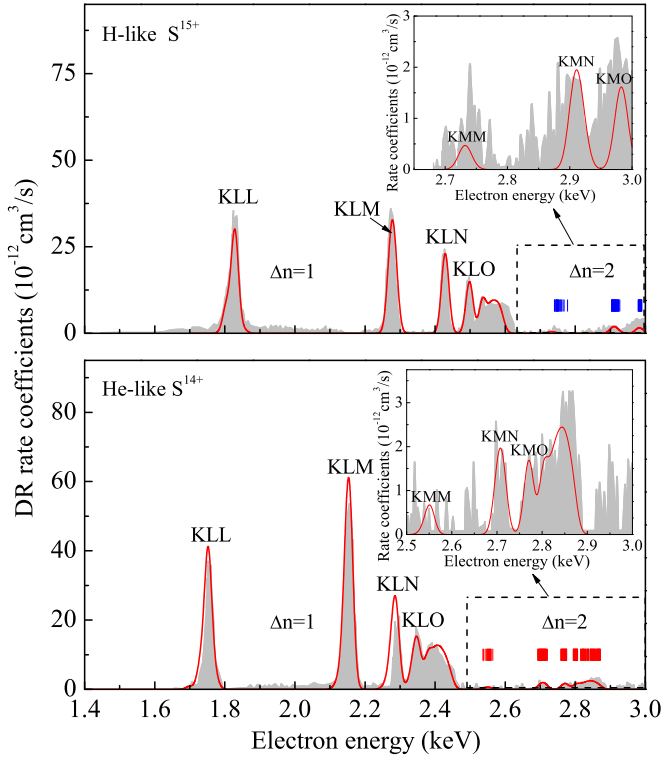
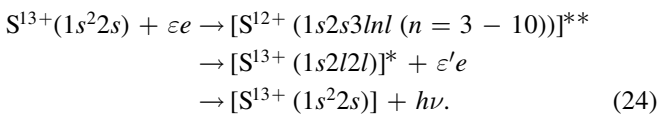
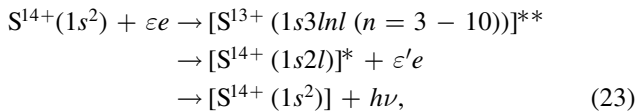
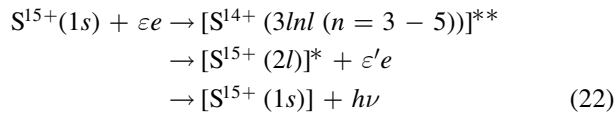


Figure 1. Partial DR rate coefficients of S^{15+} (upper panel) and S^{14+} (lower panel) ions as functions of the impact electron energy. While the experimental results (Mahmood et al. 2012) are given by the gray area, the present ones are marked by the red line, in which the experimental full width at half maximum 24 eV has been utilized. The calculated DR positions for $\Delta n = 2$ resonance are shown by vertical bars. The inset graph shows the DR rate coefficients of $\Delta n = 2$ for hydrogenlike and heliumlike sulfur ions and has the same energy scale.

present excitation energies are in excellent agreement with the results in Kramida et al. (2019). Moreover, it should be noted that since the electron-impact energies utilized in the EIE experiments range from 2.4 to 3.0 keV, the excitations from the $1s$ state to the $3l$ and even energetically higher states of S^{15+} ions as well as from the $1s$ state to the $4l$ and higher states of S^{14+} and S^{13+} ions are not considered in the calculations due to higher excitation thresholds as shown in Table 4.

In addition to those direct excitation processes as given by Equations (19)–(21), the following resonant excitation and corresponding radiative decay processes are also considered,



In Figure 3, we display the synthesized EIE rate coefficients corresponding to the direct and resonant excitation processes of S^{15+} , S^{14+} , and S^{13+} ions, i.e., Equations (22)–(24), together with the experimental results (Mahmood et al. 2012). In the

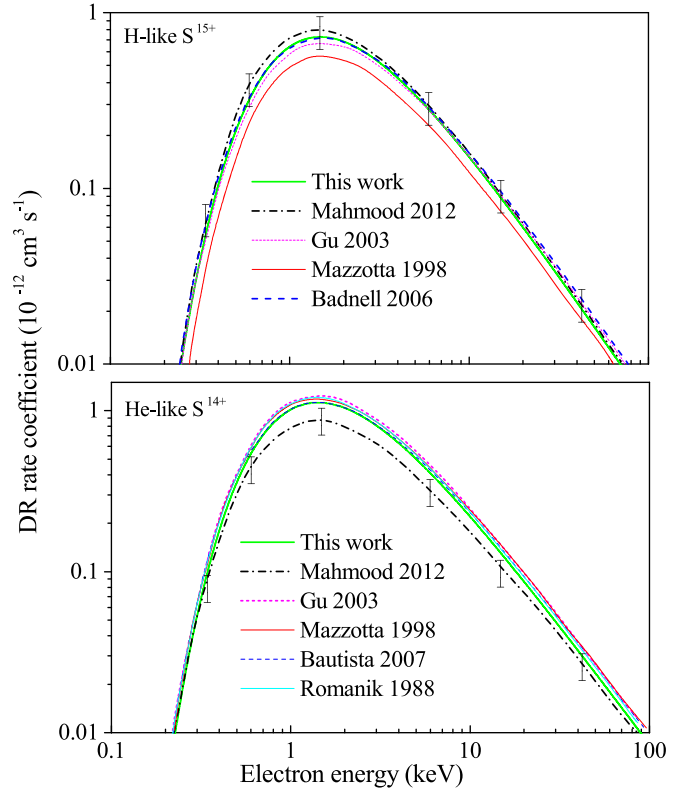


Figure 2. Comparison of total DR rate coefficients of S^{15+} (upper panel) and S^{14+} (lower panel) ions with other available experimental and theoretical results from the Romanik (1988), Mazzotta et al. (1998), Gu (2003), Badnell (2006), Bautista & Badnell (2007), and Mahmood et al. (2012).

Table 3

Fitting Parameters A_i ($10^{-12} \text{ cm}^3 \text{ s}^{-1} (\text{eV})^{3/2}$) and B_i (eV) in Equation (18) for the Presently Calculated Total DR Rate Coefficients of S^{15+} and S^{14+} Ions

i	H-like S^{15+}		He-like S^{14+}	
	A_i	B_i	A_i	B_i
1	131153.06	2456.35	126692.99	4193.83
2	1344.46	3067.63	63.50	-879.38
3	5791.65	1745.56	-106617.92	4421.30
4	-1127.26	2592.12	2.47	-1825.38
5	5.18	704.73	-28.29	-1308.74
6	52121.67	1872.50	252199.41	2082.89

calculated rate coefficients, the synthesized EIE rate coefficients are given by a solid red line, while the contribution from the direct excitation processes is plotted by the dashed blue line. The pink, red, and blue vertical bars represent the resonance positions of lithiumlike, heliumlike, and hydrogenlike ions, respectively. The first resonance peak corresponds to the resonant process of heliumlike ions. The second resonance peak mainly contains the resonant process of heliumlike and lithiumlike ions. In the latter resonance peaks, the resonance contribution of lithiumlike ions is very small. Therefore, the main contribution of the third resonance peak comes from heliumlike ions. Similarly, the last three peaks are mainly formed by the resonant process of hydrogenlike ions.

As seen clearly from Figure 3, the present EIE rate coefficients are overall in agreement with the experimental results after considering the contribution of the resonant excitation processes. However, there is a slight difference

Table 4

The Presently Calculated EIE Excitation Energies (in keV) from the Respective Ground States to the Listed Excited States of S^{15+} , S^{14+} , and S^{13+} Ions, Together with the Available Results from NIST (Kramida et al. 2019)

H-like S^{15+}			He-like S^{14+}					
Excited States	Excitation Energies		Excited States	Excitation Energies		Excited States	Excitation Energies	
	Pres.	NIST		Pres.	NIST		Pres.	NIST
$2s_{1/2}$	2.6205	2.6198	$(1s_{1/2}2s_{1/2})_1$	2.4292	2.4303	$(1s_{1/2}3p_{1/2})_0$	2.8789	2.8801
$2p_{1/2}$	2.6206	2.6197	$(1s_{1/2}2s_{1/2})_0$	2.4477	2.4481	$(1s_{1/2}3p_{1/2})_1$	2.8796	2.8802
$2p_{3/2}$	2.6236	2.6231	$(1s_{1/2}2p_{1/2})_0$	2.4458	2.4467	$(1s_{1/2}3p_{3/2})_2$	2.8799	2.8807
$3s_{1/2}$	3.1065	3.1059	$(1s_{1/2}2p_{1/2})_1$	2.4462	2.4471	$(1s_{1/2}3p_{3/2})_1$	2.8829	2.8839
$3p_{1/2}$	3.1065	3.1059	$(1s_{1/2}2p_{3/2})_2$	2.4478	2.4488	$(1s_{1/2}3d_{3/2})_1$	2.8819	2.8832
$3p_{3/2}$	3.1074	3.1067	$(1s_{1/2}2p_{3/2})_1$	2.4603	2.4606	$(1s_{1/2}3d_{3/2})_2$	2.8819	2.8832
$3d_{3/2}$	3.1074	3.1067	$(1s_{1/2}3s_{1/2})_1$	2.8749	2.8756	$(1s_{1/2}3d_{5/2})_3$	2.8821	2.8834
$3d_{5/2}$	3.1078	3.1071	$(1s_{1/2}3s_{1/2})_0$	2.8792	2.8803	$(1s_{1/2}3d_{5/2})_2$	2.8823	2.8835

Li-like S^{13+}								
Excited States	Excitation Energies		Excited States	Excitation Energies		Excited States	Excitation Energies	
	Pres.	NIST		Pres.	NIST		Pres.	NIST
$((1s_{1/2}2s_{1/2})_02s_{1/2})_{1/2}$	2.4078	2.4080	$((1s_{1/2}2p_{1/2})_12p_{3/2})_{5/2}$	2.4475	2.4469	$((1s_{1/2}2s_{1/2})_13s_{1/2})_{3/2}$	2.8179	
$((1s_{1/2}2s_{1/2})_12p_{1/2})_{1/2}$	2.4149	2.4153	$((1s_{1/2}2s_{1/2})_12p_{3/2})_1$	2.4478	2.4470	$((1s_{1/2}2s_{1/2})_13s_{1/2})_{1/2}$	2.8249	
$((1s_{1/2}2s_{1/2})_12p_{1/2})_{3/2}$	2.4154	2.4158	$((1s_{1/2}2s_{1/2})_02p_{3/2})_{3/2}$	2.4482	2.4476	$((1s_{1/2}2s_{1/2})_13p_{1/2})_{1/2}$	2.8273	2.8297
$((1s_{1/2}2s_{1/2})_12p_{3/2})_{5/2}$	2.4166	2.4170	$((1s_{1/2}2p_{1/2})_12p_{3/2})_{5/2}$	2.4613	2.4596	$((1s_{1/2}2s_{1/2})_13p_{1/2})_{3/2}$	2.8274	2.8298
$((1s_{1/2}2s_{1/2})_02p_{1/2})_{1/2}$	2.4374	2.4370	$((1s_{1/2}2p_{1/2})_02p_{3/2})_{3/2}$	2.4614	2.4597	$((1s_{1/2}2s_{1/2})_13p_{3/2})_{5/2}$	2.8278	
$((1s_{1/2}2s_{1/2})_02p_{3/2})_{3/2}$	2.4384	2.4380	$((1s_{1/2}2p_{1/2})_12p_{3/2})_1$	2.4648	2.4628	$((1s_{1/2}2s_{1/2})_13p_{3/2})_{3/2}$	2.8286	
$((1s_{1/2}2p_{1/2})_02p_{1/2})_{1/2}$	2.4459	2.4451	$((1s_{1/2}2p_{1/2})_02p_{3/2})_{3/2}$	2.4666	2.4646	$((1s_{1/2}2s_{1/2})_13p_{3/2})_{1/2}$	2.8287	
$((1s_{1/2}2p_{1/2})_02p_{3/2})_{3/2}$	2.4466	2.4460	$((1s_{1/2}2p_{1/2})_02p_{1/2})_{1/2}$	2.4812	2.4790	$((1s_{1/2}2s_{1/2})_13d_{3/2})_{1/2}$	2.8337	

Note. NIST: (Kramida et al. 2019).

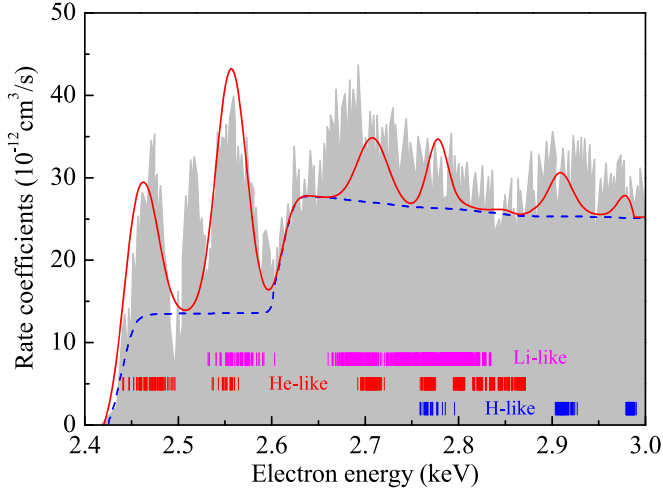


Figure 3. Synthesized EIE rate coefficients for the direct and resonant excitation processes of S^{15+} , S^{14+} , and S^{13+} ions as formulated by Equations (19)–(24). While the results for the direct excitation processes are given by the dashed blue line, the synthesized ones are marked by the solid red line. The vertical bars show calculated resonance positions.

between the theoretical and experimental results, especially for the excitation peak around the electron energy 2.52 keV. Concerning the difference between the theoretical and experimental EIE rate coefficients, it should be noted that the separate EIE rate coefficients in the experiments are not measured directly but obtained by deducting the contribution of the measured DR rate coefficients from the sum of DR and EIE rate coefficients (Mahmood et al. 2012). Since the experimental

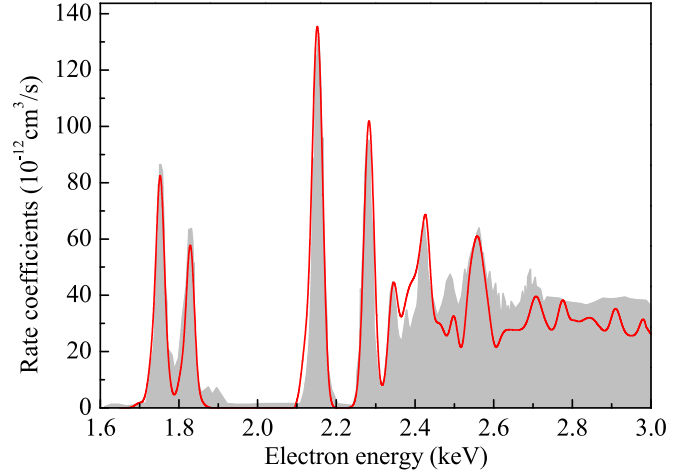


Figure 4. Presently calculated DR and EIE rate coefficients, as compared with the experimentally measured results (Mahmood et al. 2012).

results may also include contributions of other sulfur ions, such a difference could result from the ions that are not considered in the present calculations.

3.3. Synthesized DR and EIE Rate Coefficients

By means of the relevant parameters utilized in the experiments and following the theoretical procedure used in Mahmood et al. (2012), these separate theoretical rate coefficients can be employed to synthesize overall DR and EIE rate coefficients, as shown in Figure 4 together with the

corresponding experimental results for comparison. To be more specific, the overall rate coefficients are obtained by summing these separate DR and EIE rate coefficients weighted by S^{15+} , S^{14+} , and S^{13+} ion fractions determined in the experiment (Mahmood et al. 2012). The theoretically synthesized DR and EIE rate coefficients agree very well with the corresponding experimental results. Nevertheless, further studies on this topic are urgently demanded to figure out authentic reasons for the existing discrepancies in the impact energy range above 2.3 keV.

4. Conclusion

In summary, based on the experiment at the Stockholm EBIT (Mahmood et al. 2012) and the velocity distribution function of electrons, we calculate separate DR rate coefficients for S^{15+} and S^{14+} ions as well as direct and resonant EIE ones for S^{15+} , S^{14+} , and S^{13+} ions. These separate rate coefficients are further employed to synthesize the overall theoretical spectra, which are compared with the experimental results. Very good agreements are obtained except a missing excitation peak at the impact electron energy around 2.52 keV. The presently developed calculational procedure for simulating experimental DR and EIE spectra from EBIT experiments is general and can be employed to carry out similar studies.

This work is funded by the National Key Research and Development Program of China (2017YFA0402300) and the National Natural Science Foundation of China under grant Nos. 11804280, 11874051, 11864036, 11564036, and 11774292. Z. W.W. acknowledges the Scientific Research Program of the Higher Education Institutions of Gansu Province, China (grant No. 2018A-002) and Prof. Nigel R. Badnell for very helpful private communication on theoretical calculations of DR rate coefficients. R.S. acknowledges the hospitality during this stay at Northwest Normal University.

References

- Ali, S., Mahmood, S., Orban, I., et al. 2011, *JPhB*, **44**, 225203
 Anders, E., & Grevesse, N. 1989, *GeCoA*, **53**, 197
 Andersen, L. H., Hvelplund, P., Knudsen, H., & Kvistgaard, P. 1989, *PhRvL*, **62**, 2656
 Badnell, N. R., Pindzola, M. S., & Griffin, D. C. 1991, *PhRvA*, **43**, 2250

- Badnell, N. R., Spruck, K., Krantz, C., et al. 2016, *PhRvA*, **93**, 052703
 Badnell, N. R. 2006, *A&A*, **447**, 389
 Bautista, M. A., & Badnell, N. R. 2007, *A&A*, **466**, 755
 Burgess, A. 1964, *ApJ*, **139**, 776
 Cassam-Chenai, G., Decourchelle, A., Ballet, J., et al. 2004, *A&A*, **427**, 199
 Chang, J. J. 1975, *PhRvA*, **12**, 791
 Chantrenne, S., Beiersdorfer, P., Cauble, R., & Schneider, M. B. 1992, *PhRvL*, **69**, 265
 Crandall, D. H., Taylor, P. O., & Dunn, G. H. 1974, *PhRvA*, **10**, 141
 Deb, N. C., & Hibbert, A. 2006, *JPhB*, **39**, 4301
 Dyall, K. G., Grant, I. P., Johnson, C. T., Parpia, F. A., & Plummer, E. P. 1989, *CoPhC*, **55**, 425
 Foster, A. R., Smith, R. K., Brickhouse, N. S., Kallman, T. R., & Witthoef, M. C. 2010, *SSRv*, **157**, 135
 Grant, I. P. 1974, *JPhB*, **7**, 1458
 Gu, M. F. 2003, *ApJ*, **590**, 1131
 Gu, M. F. 2008, *CaPh*, **86**, 675
 Hagelstein, P. L. 1986, *PhRvA*, **34**, 874
 Hwang, U., Laming, J. M., Badenes, C., et al. 2004, *ApJL*, **615**, L117
 Ishisaki, Y., Ezoe, Y., Yamada, S., et al. 2018, *JLTP*, **193**, 991
 Kilgus, G., Berger, J., Blatt, P., et al. 1990, *PhRvL*, **64**, 737
 Kilgus, G., Habs, D., Schwalm, D., et al. 1992, *PhRvA*, **46**, 5730
 Knapp, D. A., Marrs, R. E., Levine, M. A., et al. 1989, *PhRvL*, **62**, 2104
 Kramida, A., Ralchenko, Yu., Reader, J. & NIST ASD Team 2019, NIST Atomic Spectra Database (version 5.7), <https://physics.nist.gov/asd>
 Kunze, H. J., & Johnston, W. D. 1971, *PhRvA*, **3**, 1384
 Lafyatis, G. P., & Kohl, J. L. 1987, *PhRvA*, **36**, 59
 Mahmood, S., Ali, S., Orban, I., et al. 2012, *ApJ*, **754**, 86
 Massey, H. S. W., & Bates, D. R. 1942, *RPPH*, **9**, 62
 Mazzotta, P., Mazzitelli, G., Colafrancesco, S., et al. 1998, *A&AS*, **133**, 403
 Piwiński, M., Kłosowski, Ł., Chwiroł, S., et al. 2018, *JPhB*, **51**, 085002
 Porquet, D., Dubau, J., & Grosso, N. 2010, *SSRv*, **157**, 103
 Porquet, D., Mewe, R., Dubau, J., Raassen, A. J. J., & Kaastra, J. S. 2002, *A&A*, **376**, 1113
 Pradhan, A. K., & Shull, J. M. 1981, *ApJ*, **249**, 821
 Ren, C., Wu, Z. W., Jiang, J., et al. 2018, *PhRvA*, **98**, 012711
 Romanik, C. J. 1988, *ApJ*, **330**, 1022
 Shen, T. M., Chen, C. Y., Wang, Y. S., Zou, Y. M., & Gu, M. F. 2007, *JPhB*, **40**, 3075
 Shore, B. W. 1969, *ApJ*, **158**, 1205
 Smith, R. K., Brickhouse, N. S., Liedahl, D. A., & Raymond, J. C. 2001, *ApJL*, **556**, L91
 Takahashi, T., Kokubun, M., Mitsuda, K., et al. 2018, *JATIS*, **4**, 021402
 Williams, W., & Bozinis, D. 1975, *PhRvA*, **12**, 57
 Wong, K. L., Beiersdorfer, P., Reed, K. J., & Vogel, D. A. 1995, *PhRvA*, **51**, 1214
 Wu, Z. W., Dong, C. Z., & Jiang, J. 2012, *PhRvA*, **86**, 022712
 Wu, Z. W., Jiang, J., & Dong, C. Z. 2011, *PhRvA*, **84**, 032713
 Wu, Z. W., Zhang, Y. Z., Fu, Y. B., et al. 2015, *EPJD*, **69**, 140
 Zhang, H. L., & Pradhan, A. K. 1995, *PhRvA*, **52**, 3366
 Zhang, H. L., & Sampson, D. H. 2002, *PhRvA*, **66**, 042704